

RESEARCH ARTICLE

Development of Benzimidazole Anticancer Leads for EGFR Inhibition by 3D-QSAR Based Virtual Screening, Molecular Docking, Molecular Simulation and Drug Likeness Study

Ranjeeta Verma¹, Shweta Verma² and Nahid Abbas^{3,*}

¹Research Scholar IFTM University, Moradabad, India; ²Department of Chemistry, IFTM University, Moradabad, India; ³Akshaya Institute of Pharmacy, Tumkur Affiliated to Rajiv Gandhi University of Health Science, Bengaluru, India

Abstract: Background: Breast cancer is the most common cancer in women. Tyrosine kinase inhibitors were developed to treat breast cancer. EGFR/ErbB1 inhibition has proved to be a promising target in breast carcinoma therapy. Drugs with benzimidazole nucleus **have** been approved by the FDA for cancer treatment.

Objective: To design and develop benzimidazole anticancer small molecules for EGFR inhibition for the treatment of breast cancer.

Methods: By 3D-QSAR-based virtual screening, molecular docking, molecular simulation and drug likeness study.

Results: In this research, a 3D-QSAR **pharmacophore** was generated with four salient features. Namely H-bond acceptor (HBA), two ring aromatic (RA) and hydrophobic (HY) features. Its correlation-coefficient (r) is 0.8412, RMSD of 0.96 and with 32.84 bits cost difference value. With virtual screening, 4 top hits were identified. Novel benzimidazole derivatives were designed (1a-1l) by using the features of hit molecules and the pharmacophore. The novel designed small molecules **that** were druggable as they passed the Lipinski and Veber rule. Novel ligands and EGFR protein interaction **were** good. 1a and 1i were found to be the best-designed molecules. They had -8.6 Kcal/mol and -8.4 Kcal/mol docking interaction energy, respectively, whereas Compound 4 (reference) scored -7.4 Kcal/mol. Both these molecules were stable inside the binding pocket of the EGFR protein. The molecular dynamic simulation study revealed that 1a attained equilibrium at 0.15nm.

Conclusion: In silicon novel benzimidazole small molecules were designed and developed as EGFR inhibitors to treat breast cancer.

Keywords: EGFR, breast cancer, pharmacophore, simulation, docking, benzimidazole.

1. INTRODUCTION

Cancer is a disease which led to 9.6 million deaths in the previous decades [1]. It is reported that females suffer from breast, stomach, liver, bone, lung, colon leukemia, and cervical cancer [2]. World Health Organization (WHO) states that cancer has increased mortality worldwide [3]. Among 19.3 million cases of reported cancers in 2020, 2.3 million were breast cancer cases [4].

Chemotherapy, hormone therapy, radiotherapy, surgical removal, and immunotherapy are used in the treatment of cancer. Currently, many small molecules have been

developed to treat this disease [5-8]. Recently, benzimidazole derivatives have been developed into anticancer drugs.

The benzimidazole nucleus has minimal toxicity; hence, it is an excellent scaffold for the development of anticancer agents. Benzimidazole (also known as 1*H*-benzimidazole, 1,3-benzodiazole, benzoglyoxaline, iminazole, and imidazole) is made up **of** an aromatic benzene ring fused with an imidazole ring at 4,5-position. The proton on the first Nitrogen exhibits tautomerism after aprotic solvent interaction [9, 10]. Among the US Food and Drug Administration (FDA) approved drug benzimidazole heterocycle is among the top ten [11].

Anticancer agents with benzimidazole ring have been reported. They are categorized as DNA intercalation and alkylating agents, androgen receptor antagonists, and inhibitors of poly(ADP-ribose) polymerase (PARP), topoisomer-

*Address correspondence to this author at the Akshaya Institute of Pharmacy, Tumkur Affiliated to Rajiv Gandhi University of Health Science, Bengaluru, India; E-mail: nahid.is.abbas@gmail.com

ase, protein kinase, dihydrofolate reductase and microtubule [12, 13].

Some of the well-known drugs having benzimidazole scaffold are displayed in Table 1 with their biological targets and uses [14].

1.1. Epidermal Growth Factor Receptor (EGFR/HER-1)

The epidermal growth factor receptor (EGFR/HER-1) is the most prioritized molecular cancer target. EGFR is **over-expressed** in tumor cells. EGFR is a member of the ErbB/EGFR family of tyrosine kinase **receptors**. It gives **signals** to cells, which are activated by heregulin-like EGFR ligands, for cell proliferation in homeostasis [15]. The growth factor ligands (*i.e.* EGF) bind to EGFR and make an active homodimer. After EGFR dimerization (homo or hetero-dimerization), it stimulates intrinsic intracellular tyrosine kinase. This leads to downstream activation followed by signaling through phosphotyrosine binding (SH2) domains. Signaling pathways, like mitogen-activated protein kinase (MAPK), Protein kinase B (Akt) and Jun N-terminal kinase (JNK); such proteins alter phenotypes such as cell migration, adhesion and cell proliferation [16, 17].

The role of the ErbB family in breast carcinoma has led to the development of Abemaciclib, Lapatinib, Erlotinib, Imatinib and other tyrosine kinase inhibitors. FDA-approved EGFR/ErbB1 inhibitors are used to treat breast cancer, non-small cell lung cancer and chronic myeloid leukemia [18]. Imatinib used in chronic myeloproliferative diseases exhibit cardiotoxicity [19].

Lapatinib acts as a dual inhibitor of EGFR and HER2 tyrosine kinases and is used in metastatic breast cancer chemotherapy [20]. Erlotinib and Gefitinib produce skin rashes [21]. Many protein tyrosine kinase inhibitors exhibit poor bioavailability. Thus, there is a requirement for novel anticancer agents with better oral bioavailability and low toxicity profile.

In the current research work, novel small molecules with a benzimidazole **core that have** better ADMET properties, are designed for EGFR inhibition, using 3D-QSAR pharmacophore-based virtual screening, docking and molecular dynamic simulation studies.

2. MATERIALS AND METHODS

2.1. 3D-QSAR Pharmacophore Development

All compounds were drawn with Chem Draw Ultra 12.0 Using Accelrys Discovery Studio 3.5 (DS 3.5) window, and its CHARMM force field 3D-QSAR pharmacophore was produced. The H-bond acceptor (HBA), ring aromatic (RA) and hydrophobic (HY) were the main features. With 255 conformations, 20.0 kcal/mol energy, 0.3 weight, 3 uncertainty, 1.5 Å inter-feature spacing, the training set comprised of small molecules enlisted in Table 1. The HypoGen algorithm of DS 3.5 produced 10 **hypotheses** and were analyzed by cost analysis. The summation of the weight, error, and configuration costs made up the total cost. The root mean square (rms) difference between the estimated and predicted activity of the training set molecules influenced the error cost, which counter **affects** the total cost. The pharmaco-

phore model was further validated using cost analysis, Fischer's test and external test set validation [22].

2.2. Virtual Screening of Chemical Database

A pharmacophore-based virtual screening of the ZINC database was done. The validated pharmacophore model was used as an input query to search for potential hits from 727842 molecules of the ZINC database using the 'Flexible search' tool in DS software.

Among the screened molecules, the top hit structural configuration was studied. Its features were incorporated to design novel molecules as EGFR inhibitors. These newly designed molecules were studied for drug likeliness, docking and simulation studies. In the context of molecular docking experiments, the charges on both the proteins and ligands were explicitly considered to ensure accurate docking interactions. The proteins were prepared by assigning partial atomic charges based on the CHARMM27 force field, while the ligands were optimized and assigned charges using the Gasteiger method.

2.3. Molecular Docking

2.3.1. Protein Preparation

The 3D structure of the protein EGFR kinase with the PDB ID: 3W2S was downloaded from the Protein Data Bank *via* the Protein Preparation Wizard in Maestro. Several pre-processing steps were applied to the protein, including assigning bond orders, removing original hydrogens, adding hydrogens, establishing zero-order bonds to metals, forming disulfide bonds, converting seleno-methionines to methionines, addressing missing side chains and loops through Prime, eliminating water molecules farther than 5 Å from hetero groups, and generating hit states using Epik at pH 7.0 ± 2.0. Subsequently, the protein underwent refinement employing PROPKA at pH 7.0, and **its structure was optimized**. The protein was further subjected to restrained minimization utilizing the OPLS3 force field as described in previous works.

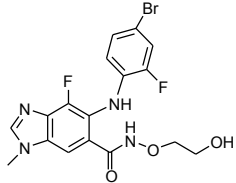
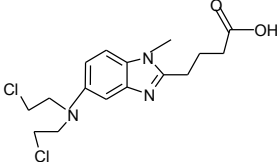
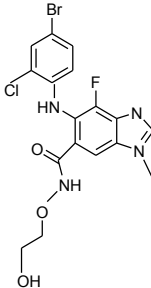
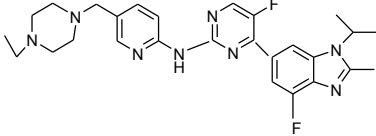
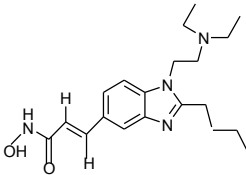
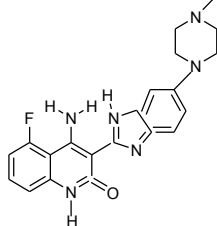
2.3.2. Receptor Grid Generation

Following protein preparation, a receptor grid was created. This grid was centered on the active site, using the co-crystallized ligand as the reference point. The grid box used for docking was meticulously designed with dimensions of 20 Å × 20 Å × 20 Å to encapsulate the active site and its surrounding residues, ensuring sufficient space for ligand flexibility. The grid center was set at 1.7, 0.72, and 12.31 Å coordinates, which corresponded to the centroid of the identified binding site. Amino acid residues critical for grid generation were identified based on their proximity to the binding pocket, including GLY719, SER720, LYS867, LEU989, and PRO990. These residues were selected to ensure precise localization of the grid box while encompassing all potential interaction regions.

2.3.3. Preparation of Ligand

All molecules were drawn, converted into 3D structures, and subjected to energy minimization using the Ligprep and

Table 1. Structures, biological targets and applications of clinically approved drugs with benzimidazole scaffold (training set for pharmacophore) as found in <https://www.drugs.com/>.

| Compound Code | Structure | Current status | Target | Application |
|--|---|------------------|--|--|
| Binimetinib (NCT04965818 and NCT03170206) |  | sold as Mektovi | Mitogen-activated protein kinase inhibitor IC ₅₀ = 12 nM | Metastatic melanoma with specific mutations |
| sBendamustine (NCT04217317 and NCT04510636), |  | Sold as Treanda | It is an <i>alkylating agent</i> . IC ₅₀ = 50 μM | Treats chronic lymphocytic leukemia |
| Selumetinib (NCT02768766) |  | Sold as Koselugo | It is a selective, non-ATP-competitive oral MEK1/2 inhibitor IC ₅₀ = 14 nM | Treats neurofibromatosis type 1 |
| Abemaciclib (NCT04003896 and NCT04040205) |  | Sold as Verzenio | It is more selective toward CDK4 IC ₅₀ = 2 nM than CDK6 IC ₅₀ = 25 nM | Treats HR-positive and HER2-negative breast cancer |
| Pracinostat (NCT03848754), |  | Phase III trial | Pracinostat (SB939) is a potent pan-HDAC (histone deacetylase) inhibitor with IC ₅₀ = 40 nM | Treats advanced solid tumors and AML |
| Dovitinib (NCT01635907), |  | Phase II trial | potent multi-targeted tyrosine kinase (RTK) inhibitor with IC ₅₀ = 27 nM | Treats AML |

Confgen functions within Maestro. The resulting library was then saved in the maegz format.

2.3.4. Molecular Docking

Next, molecular docking was conducted using the Glide program with the Standard Precision (SP) algorithm to assess the interactions between proteins and ligands and determine their binding affinities. To validate the molecular docking, a re-docking procedure was performed with the co-crystallized ligand placed within the grid.

2.4. Molecular Dynamic Simulation

Molecular dynamics (MD) simulation was carried out using GROMACS 2022.2. The following steps were done.

2.4.1. Preparation of Enzyme

The 3-dimensional (3D) models of ligand-protein complexes were exported to .pdb format using Pymol. The dynamic behavior of the complexes was evaluated using molecular dynamic (MD) simulation in the GROMACS pack-

age program (version 2022.2) [23-25]. Protein topology was constructed by pdb2gmx with the CHARMM27 force field [26], and ligand topology was generated using the SwissParam server [27].

2.4.2. Setting Up the System for Simulation

After force field application, the complexes were inserted into the system. They were solvated with the TIP3P water model [28] in a cubic box greater than 1 nm from the edge of the protein. Na⁺ ions were added, and energy minimization was done using the steepest descent algorithm. Next, 100 ps of NVT simulation at 300 K and 100 ps of NPT simulation will be used to equilibrate the entire system. Leapfrog algorithm was employed in the constant-temperature, and pressure (NPT) for protein, ligand, water molecules, and ions [29]. The Berendsen temperature and pressure coupling constants were set to .1 and 2, respectively, to keep the system in a stable environment (300 K temperature and 1 bar pressure) [30]. Finally, MD simulation for 100 ns was performed. The pressure coupling with time-constant was set at 1 ps in the LINCS algorithm [31] was used. The Van der Waals and Coulomb interactions were truncated at 1.2 nm, and the PME algorithm [32] built into GROMACS was used to minimize the error from truncation.

2.4.3. Visualization and Analysis of Simulation

The trajectory files are visualized through VMD (Visual Molecular Dynamics) 1.9.2. [33] and analyzed by HeroMDAnalysis [34, 35] and Xmgrace 5.1.25 tool [36].

2.5. Drug Likeness Protocol

Discovery Studio 3.5 was used to predict the drug-likeness property of the newly designed compounds with the help of the Lipinski drug filter tool.

3. RESULTS AND DISCUSSION

3.1. 3D-QSAR Pharmacophore

The best pharmacophore with a correlation coefficient (r) of 0.8412, RMSD of 0.96, and an acceptable cost difference value (32.84 bits) between the total and the null cost was selected. This pharmacophore model had one HBA, two RA and one hydrophobic (HY-1). This pharmacophore, along with their inter-feature distance, is shown in Fig. (1).

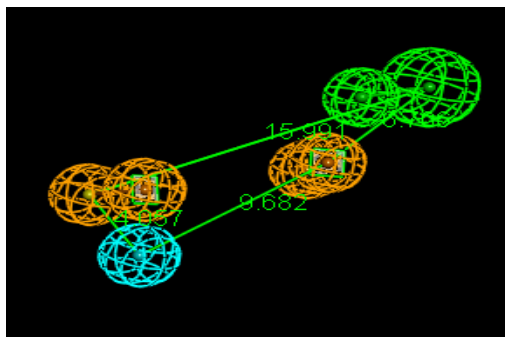


Fig. (1). Best 3D-QSAR pharmacophore, H-bond acceptor (HBA) shown as green, ring aromatic (RA) shown as orange and hydrophobic (HY) shown as cyan. (A higher resolution / colour version of this figure is available in the electronic copy of the article).

3.2. Virtual Screening

With this pharmacophore, a hit list of 995 compounds matching the pharmacophore model was obtained from 727842 compounds. Molecules with an estimated IC₅₀ below 50 nM were considered active new hits. A set of 493 hits were obtained. After Lipinski's drug-likeness screening, 23 molecules were identified. After molecular docking, 4 top hits were found, which are displayed in Table 2 and Fig. (2) displays the steps for virtual screening. Four top hits were retrieved from the ZINC database after the whole virtual screening procedure. The retrieved molecules belonged to the class of 6-Furan-2-yl-9-(4-methoxy-benzyl)-9H-purin-2-ylamine (ZINC2 8523512); 1H-benzimidazol-2-yl)-carbamic acid methyl ester (ZINC00043475); Benzofuran-2yl-(4-chloro-phenyl)methanol (ZINC00000176) and (Bromo-4-imidazol-1-yl-phenyl)-2-cyano-2-dimethyl-thioacetamide (ZINC00005786).

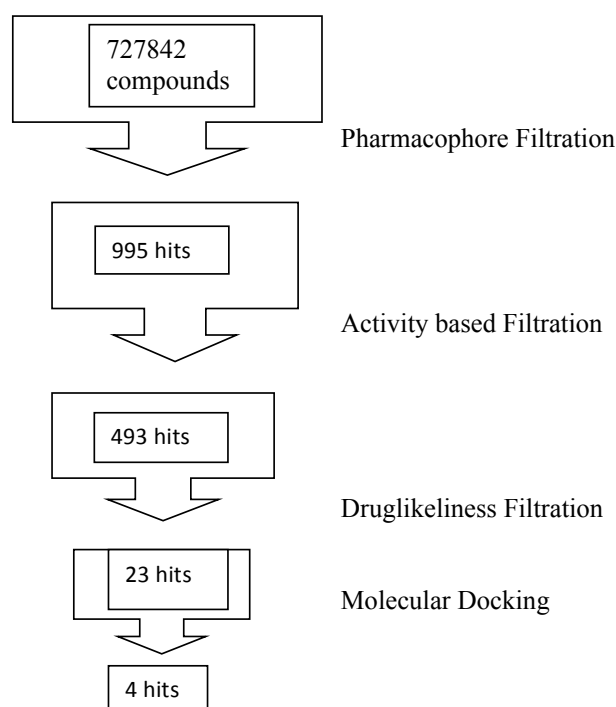


Fig. (2). Steps for virtual screening.

By studying the features of these molecules and by incorporating the pharmacophore features novel molecules were designed with a benzimidazole nucleus. Their ADMET parameters were studied. Table 3 displays the newly designed novel molecules with the ADMET. Fig. (3) displays the perfect fit of novel molecules in the designed 3D-QSAR pharmacophore. The novel-designed benzimidazole molecules passed the Lipinski rule, were orally bioavailable and were not hepatotoxic.

3.3. Molecular Docking

The designed molecules were docked. The docking score is displayed in Table 4. They were binding in the active site amino acids.

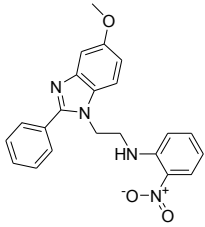
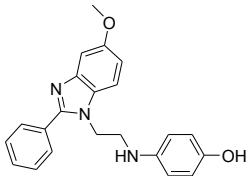
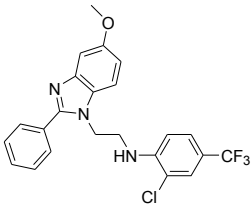
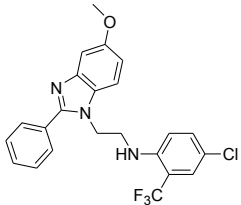
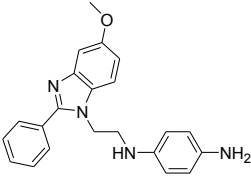
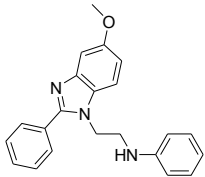
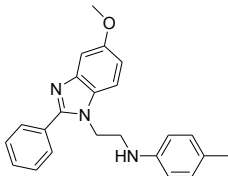
Table 2. Top hit molecules.

| | | | |
|--------------|--------------|--------------|--------------|
| | | | |
| ZINC28523512 | ZINC00043475 | ZINC00000176 | ZINC00005786 |

Table 3. Designed novel molecules and ADMET parameters.

| Structures | Mol Wt | H-Bond Donor | H-Bond Acceptor | TPSA | LogP | GI Absorption | Oral Bioavailability | CYP1A2 Inhibition |
|------------|--------|--------------|-----------------|-------|------|---------------|----------------------|-------------------|
| | 456.42 | 1 | 6 | 64.19 | 5.75 | 1 | 0.7 | 0.71 |
| | 475.12 | 0 | 5 | 61.19 | 5.64 | 1 | 0.79 | 0.5 |
| | 443.48 | 1 | 5 | 39.08 | 6.44 | 1 | 0.8 | 0.94 |
| | 474.76 | 1 | 4 | 39.08 | 6.30 | 1 | 0.84 | 39.08 |
| | 357.4 | 1 | 4 | 39.08 | 5.13 | 1 | 0.85 | 0.98 |

(Table 3) Contd....

| Structures | Mol Wt | H-Bond Donor | H-Bond Acceptor | TPSA | LogP | GI Absorption | Oral Bioavailability | CYP1A2 Inhibition |
|---|--------|--------------|-----------------|-------|------|---------------|----------------------|-------------------|
|  1f | 388.4 | 1 | 6 | 82.12 | 4.73 | 1 | 0.7 | 0.92 |
|  1g | 358.44 | 1 | 4 | 47.26 | 5.05 | 1 | 0.57 | 0.92 |
|  1h | 445.8 | 1 | 4 | 39.08 | 6.5 | 1 | 0.8 | 0.91 |
|  1i | 445.87 | 1 | 4 | 39.08 | 6.5 | 1 | 0.75 | 0.95 |
|  1j | 358.45 | 2 | 5 | 65.16 | 4.41 | 1 | 0.81 | 0.96 |
|  1k | 343.43 | 1 | 4 | 39.08 | 4.48 | 1 | 0.80 | 0.99 |
|  1l | 357.4 | 1 | 4 | 39.08 | 5.13 | 1 | 0.85 | 0.98 |

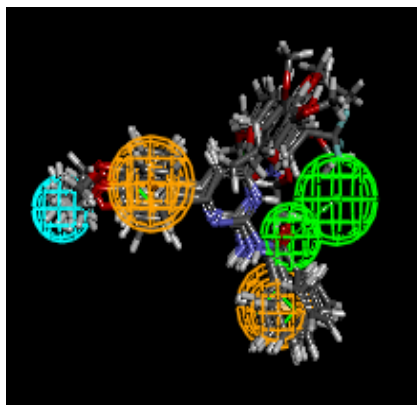


Fig. (3). The designed novel benzimidazole molecules with a perfect fit in the pharmacophore. (A higher resolution / colour version of this figure is available in the electronic copy of the article).

Table 4. Molecular docking studies of various molecules inside the active site of EGFR kinase (PDB ID: 3W2S).

| Ligand | Interaction Energy (Kcal/mol) | H Bonds | Amino acids |
|------------------------|-------------------------------|---------|---|
| 1a | -8.6 | 1 | hbond interaction with ASP800, hydrophobic interactions with LEU718, ALA722, CYS797, LEU844 |
| 1b | -8.3 | 1 | Arg705 |
| 1c | -8.1 | 2 | Arg705, Arg297 |
| 1d | -8.1 | 1 | Arg705 |
| 1e | -8.2 | 0 | - |
| 1f | -8.2 | 1 | Arg705 |
| 1g | -7.9 | 3 | Arg705, Asn298 |
| 1h | -8.0 | 0 | - |
| 1i | -8.4 | 3 | hbond interaction with ASP800, hydrophobic interactions with LEU718, VAL726, CYS797, PHE997 |
| 1j | -8.1 | 1 | Arg705 |
| 1k | -8.0 | 1 | Arg705 |
| 1l | -8.3 | 0 | - |
| Compound 4 (Reference) | -7.5 | 3 | Hbond ASP800, THR854 |

The Standard Precision (SP) docking showed that 2 compounds have exhibited strong interactions with the catalytic

residues within the active site of the EGFR kinase. These interactions were hydrogen bond and hydrophobic interactions. Compound 1a and Compound 1i were selected for further investigation through molecular dynamics studies with EGFR kinase (PDB ID: 3W2S) (Fig. 4).

3.4. Molecular Dynamic Simulations of EGFR Kinase in Complex with Ligands, Compound 1a and Compound 1i

To understand the conformational changes and evaluate the binding of molecules, Compound 1a and Compound 1i against EGFR kinase (PDB ID: 3W2S), MD simulations were done for a period of 100 ns for two models, namely, Compound 1a-EGFR kinase complex, and Compound 1i-EGFR kinase complex (Fig. 5). Their simulations were evaluated by studying parameters like Root-Mean-Square-Deviation (RMSD), Root-Mean-Square-Fluctuation (RMSF), h-bond interactions, and its % occupancies over time.

3.4.1. RMSD Analysis

The protein-RMSD was evaluated during the simulation. The multiplot for protein C α versus time for 2 simulations is shown in Fig. (6). Both the complexes have attained a plateau in RMSD values (of less than 0.3 nm), so both the protein-ligand complexes were stable during the simulation. The ligand is also stable with the protein and its binding pocket. Both ligands 1a and 1i have displayed significant stable deviation. Compound 1a has attained an equilibrium value of around 0.15 nm, while ligand 1i has displayed a slight distress with the RMSD value of 0.25 nm. The ligand RMSD values indicated that these ligands had good binding with the proteins.

3.4.2. RMSF Analysis

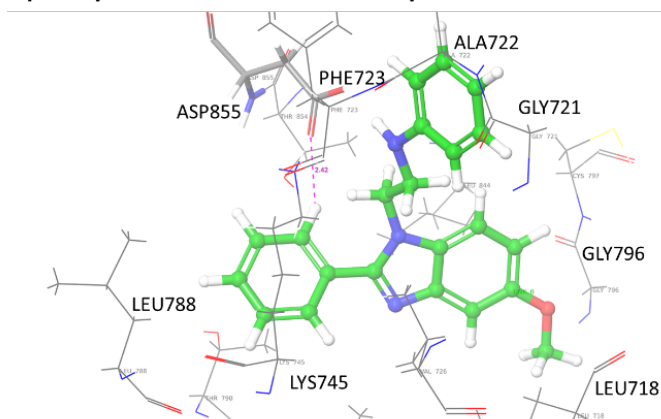
The Protein-RMSF is used in the characterization of local changes along the protein chain. The multiplot for protein-RMSF (nm) versus residue number is shown in Fig. (7). Notably, the plot describes fluctuation of less than 0.5 nm for the EGFR kinase in complex with Compound 1a and 1i. It can be concluded that ligand binding has brought stability to conformation of the protein.

3.4.3. H-bond Interaction

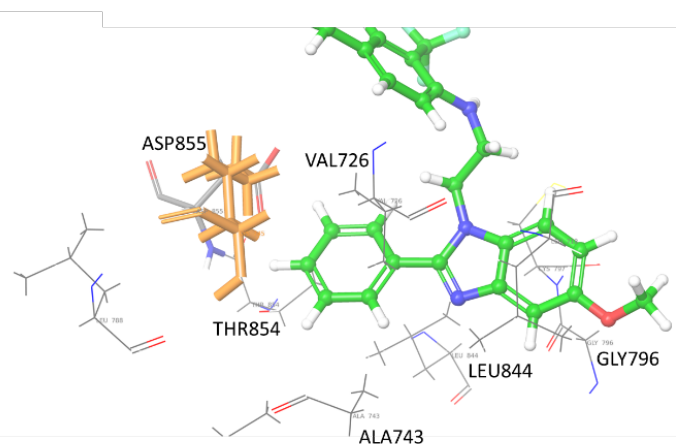
Molecular interactions, particularly the H-bond interactions, are distance and angle dependent and are liable to disrupt under dynamic conditions. Herein, analysis of both the ligand-protein complexes was done. The plot for the number of hydrogen vs time is given in Fig. (8). From the plot, it is observed that Compound 1a, and Compound 1i have displayed an average of 1-3 H-bond during the simulation. To access the residues involved in such interactions and their stabilities, the % occupancies vs the residues were also calculated.

Fig. (9) represents the histogram of % occupancies of the H-bond formed by the two ligands. This figure illustrates the capacity of the ligand Compound 1a to establish stable interactions with EGFR kinase residues PRO990 and LEU989, with occupancies of 9.87% and 5.42%, respectively. On the other hand, the ligand Compound 1i displayed significant

A) Compound 1a-EGFR kinase complex



B) Compound 1i-EGFR kinase complex



C) Compound 4-EGFR kinase complex (Reference)

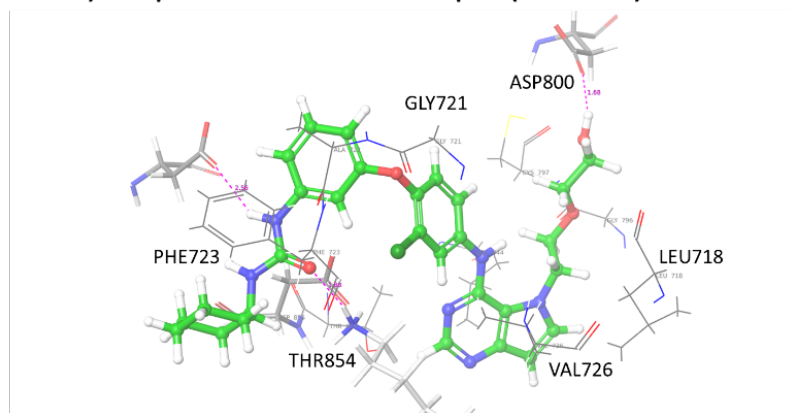
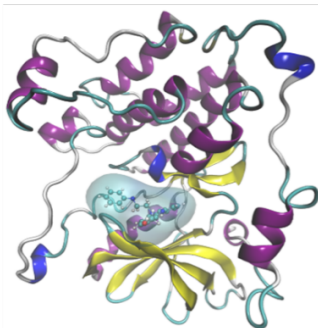


Fig. (4). Molecular docking studies reveal the binding orientations of molecules (A) Compound 1a, (B) Compound 1i, and (C) Compound 4 (reference) within the active site of the EGFR kinase (PDB ID: 3W2S). The ligand molecules are depicted in a bold stick representation, with carbon atoms in green, while interacting residues within a 4.0 Å radius are shown using stick and wire representations, with carbon atoms in grey. Hydrogen-bonding interactions are indicated by magenta dotted lines, along with the corresponding distances in angstroms (Å). (A higher resolution / colour version of this figure is available in the electronic copy of the article).

A) Compound 1a-EGFR kinase complex



B) Compound 1i-EGFR kinase complex

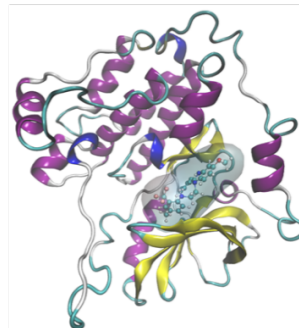


Fig. (5). Graphical representation of protein-ligand complexes: (A) Compound 1a-EGFR kinase and (B) Compound 1i-EGFR kinase, where protein is shown in cartoon representation and the ligand is shown in bond representation with transparent surface. (A higher resolution / colour version of this figure is available in the electronic copy of the article).

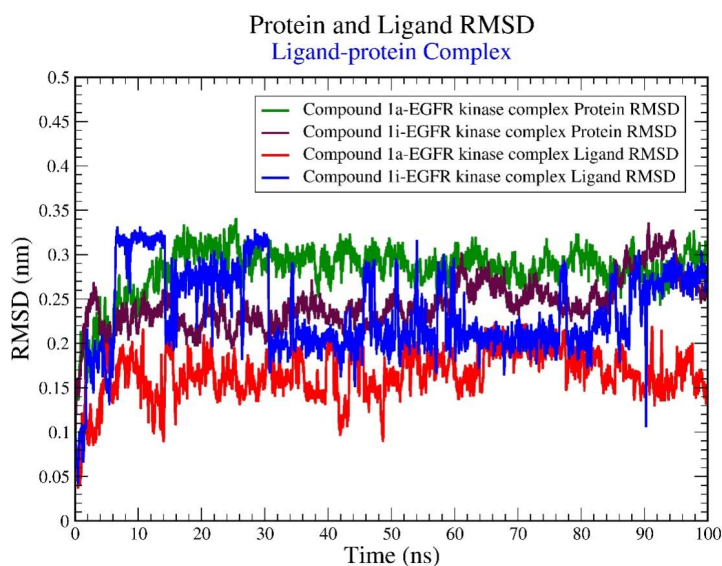


Fig. (6). Graphical representation of the plots showing protein C α and ligand RMSD (nm) versus time (100 ns) for (A) Compound 1a-EGFR kinase Protein RMSD (green), (B) Compound 1i-EGFR kinase Protein RMSD (maroon in color), (C) Compound 1a-EGFR kinase Ligand RMSD (red), and (D) Compound 1i-EGFR kinase Ligand RMSD (blue). (A higher resolution / colour version of this figure is available in the electronic copy of the article).

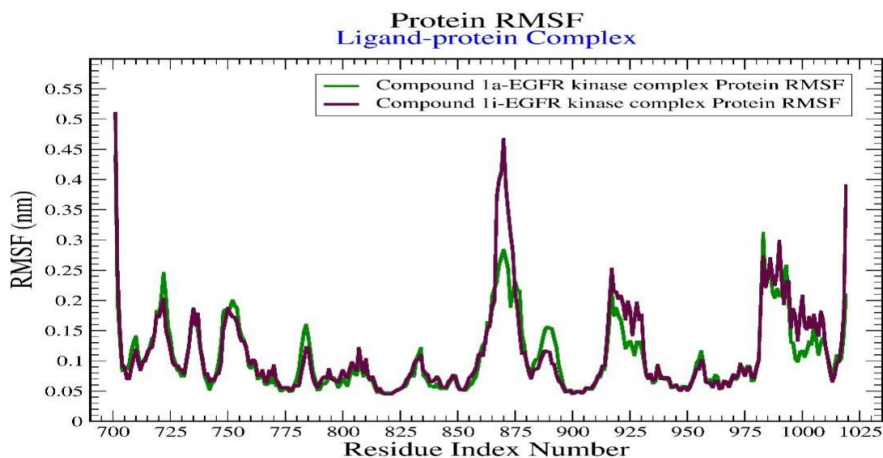


Fig. (7). Graphical representation of the plots showing the protein RMSF (nm) versus residue index number of protein for (A) Compound 1a-EGFR kinase Protein RMSF (green in color), and (B) Compound 1i-EGFR kinase Protein RMSF (maroon in color). (A higher resolution / colour version of this figure is available in the electronic copy of the article).

hydrogen bond interactions with residues SER720, LYS867, and GLY719, which remained stable for 26.44%, 11.39%, and 9.43% of the simulation duration, respectively. In summary, both ligands exhibit the potential to bind to EGFR kinase, but Compound 1i appears to be the more efficient ligand.

3.4.4. MMGBSA Calculations

The molecular dynamics study included an in-depth evaluation of binding energetics through MMGBSA calculations. Binding free energy (ΔG) values were computed for both ligands at various stages of the simulation (0, 50, and 100 ns). The average ΔG values for Compounds 1a and 1i indicated favorable binding within the EGFR active site, as presented in Table 5 and Fig. (10). These findings highlight the potential of Compounds 1a and

1i as promising candidates for further pharmacological investigations, particularly in the context of cancer therapy.

CONCLUSION

In this research work, 3D-QSAR pharmacophore was generated, and virtual screening was done. The top four hit molecules were identified. Considering their properties and the pharmacophore model, novel benzimidazole derivatives were designed as EGFR inhibitors. Their ADMET values were calculated. Docking studies were performed. The novel molecules 1a and 1i had the best interaction energy and were stable inside the binding pocket as per the molecular dynamic simulation study. In summary, both ligands 1a and 1i exhibit the potential to bind to EGFR kinase, their interaction energy better than Erlotinib, but Compound 1i appears

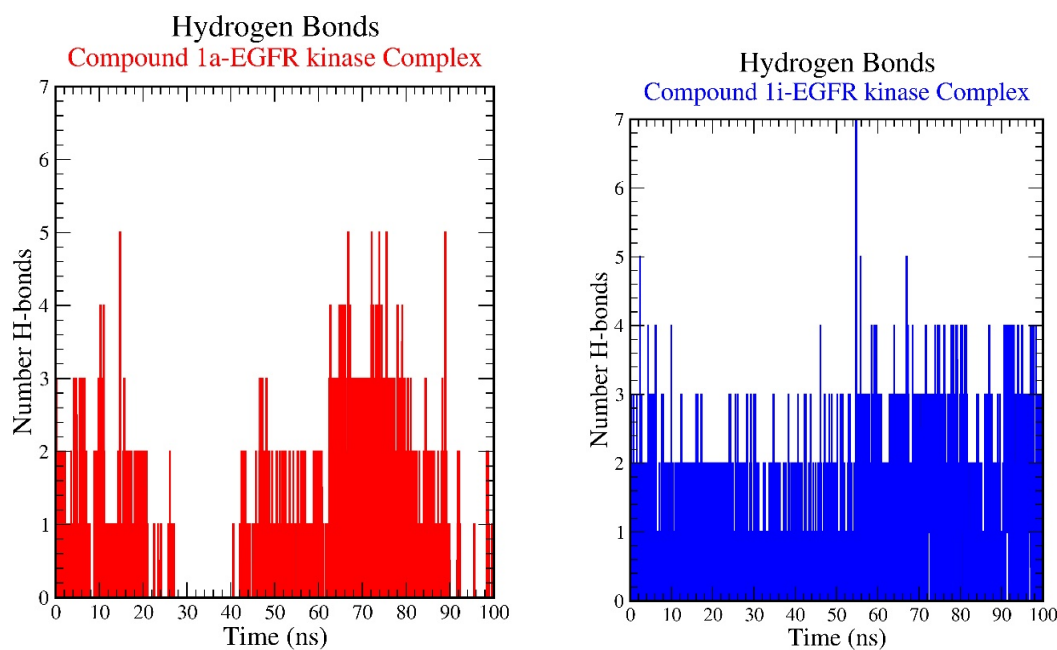


Fig. (8). Pictorial representation of the number of h-bond contacts formed by ligands, (A) Compound 1a (red in color), and (B) Compound 1i (blue in color) in complex with EGFR kinase. (A higher resolution / colour version of this figure is available in the electronic copy of the article).

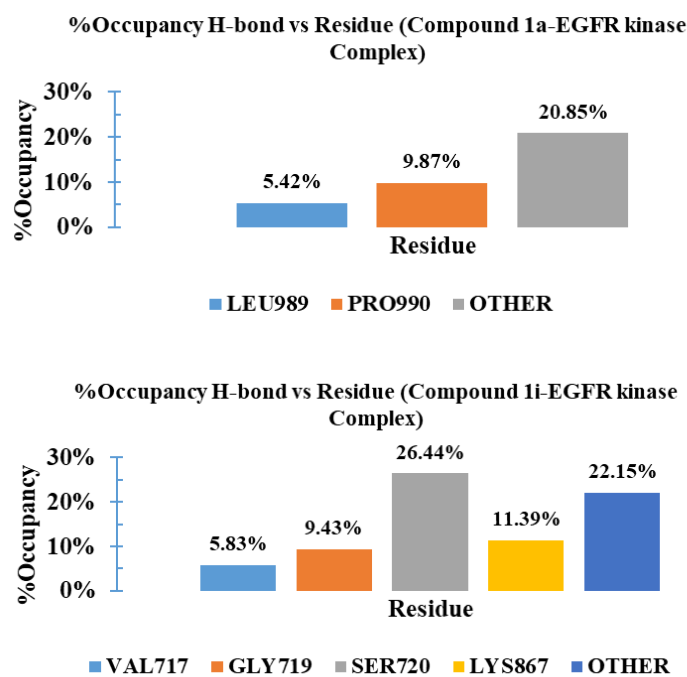


Fig. (9). Histogram representation of %occupancies of the h-bond protein-ligand contacts of (A) Compound 1a and (B) Compound 1i in complex with EGFR kinase. (A higher resolution / colour version of this figure is available in the electronic copy of the article).

Table 5. MMGBSA ΔG binding energy calculations for compound 1a and 1i in complex with EGFR (PDB ID: 3W2S).

| Ligand-protein Complex | 0 ns | 50 ns | 100 ns | Average |
|---------------------------------|--------|--------|--------|---------|
| Compound 1a-EGFR kinase complex | -33.42 | -44.54 | -42.63 | -40.20 |
| Compound 1i-EGFR kinase complex | -32.45 | -33.54 | -37.5 | -34.50 |

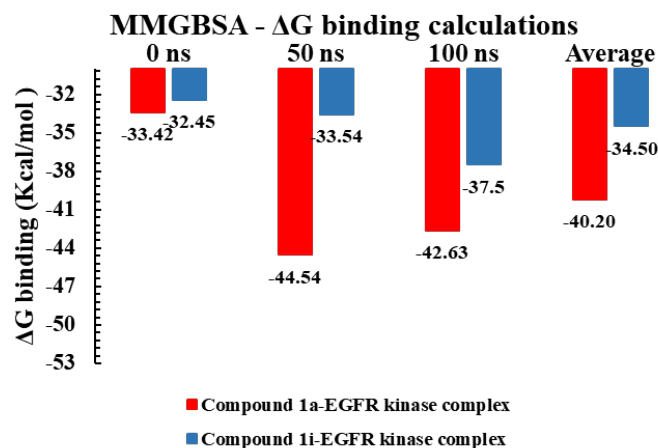


Fig. (10). MMGBSA ΔG binding energy calculations for Compound **1a** and **1i** in complex with EGFR (PDB ID: 3W2S). (A higher resolution / colour version of this figure is available in the electronic copy of the article).

to be the most promising ligand. For further investigation, in our upcoming research, these benzimidazole derivatives will be synthesized and anticancer studies will be performed.

AUTHORS' CONTRIBUTIONS

The authors confirm their contribution to the paper as follows: study conception and design were contributed by NA, data analysis or interpretation were presented by SV and RV wrote the paper. All authors reviewed the results and approved the final version of the manuscript.

LIST OF ABBREVIATIONS

| | | |
|------|---|----------------------------------|
| 3D | = | 3-dimensional |
| FDA | = | Food and Drug Administration |
| HBA | = | H-bond Acceptor |
| JNK | = | Jun N-terminal Kinase |
| MAPK | = | Mitogen-activated Protein Kinase |
| MD | = | Molecular Dynamics |
| RA | = | Ring Aromatic |
| RMSD | = | Root-mean-square-deviation |
| RMSF | = | Root-mean-square-fluctuation |
| SP | = | Standard Precision |
| WHO | = | World Health Organization |

ETHICS APPROVAL AND CONSENT TO PARTICIPATE

Not applicable.

HUMAN AND ANIMAL RIGHTS

No animals/humans were used for studies that are the basis of this research.

CONSENT FOR PUBLICATION

Not applicable.

AVAILABILITY OF DATA AND MATERIALS

All data generated or analyzed during this study are included in this published article.

FUNDING

None.

CONFLICT OF INTEREST

The authors declare no conflict of interest, financial or otherwise.

ACKNOWLEDGEMENTS

Declared none.

REFERENCES

- Kyriakopoulou, K.; Kefali, E.; Piperigkou, Z.; Bassiony, H.; Karamanos, N.K. Advances in targeting epidermal growth factor receptor signaling pathway in mammary cancer. *Cell. Signal.*, **2018**, *51*, 99-109.
<http://dx.doi.org/10.1016/j.cellsig.2018.07.010> PMID: 30071291
- Klein, S.L.; Flanagan, K.L. Sex differences in immune responses. *Nat. Rev. Immunol.*, **2016**, *16*(10), 626-638.
<http://dx.doi.org/10.1038/nri.2016.90> PMID: 27546235
- World Health Organization. Available from: <http://who.int/data/gho/data/themes/mortality-and-global-health-estimates/> (Accessed on 21 July 2021).
- Sung, H.; Ferlay, J.; Siegel, R.L.; Laversanne, M.; Soerjomataram, I.; Jemal, A.; Bray, F. Global cancer statistics 2020: GLOBOCAN estimates of incidence and mortality worldwide for 36 cancers in 185 countries. *CA Cancer J. Clin.*, **2021**, *71*(3), 209-249.
<http://dx.doi.org/10.3322/caac.21660> PMID: 33538338
- Baskar, R.; Lee, K.A.; Yeo, R.; Yeoh, K.W. Cancer and radiation therapy: Current advances and future directions. *Int. J. Med. Sci.*, **2012**, *9*(3), 193-199.
<http://dx.doi.org/10.7150/ijms.3635> PMID: 22408567
- Baloch, S.K.; Ling, L.J.; Qiu, H.Y.; Ma, L.; Lin, H.Y.; Huang, S.C.; Qi, J-L.; Wang, X-M.; Lu, G-H.; Yang, Y-H. Synthesis and

- biological evaluation of novel shikonin ester derivatives as potential anti-cancer agents. *RSC Advances*, **2014**, 4(67), 35588-35596. <http://dx.doi.org/10.1039/C4RA05610H>
- [7] Wang, X.; Su, H.; Chen, C.; Cao, X. Synthesis and biological evaluation of peptidomimetics containing the tryptamine moiety as a potential antitumor agent. *RSC Advances*, **2015**, 5(20), 15597-15602. <http://dx.doi.org/10.1039/C4RA16949B>
- [8] Liang, X.J.; Chen, C.; Zhao, Y.; Wang, P.C. Circumventing tumor resistance to chemotherapy by nanotechnology. In: *Multi-Drug Resistance in Cancer*; Humana Press, **2010**; pp. 467-488.
- [9] Wright, J.B. The chemistry of the benzimidazoles. *Chem. Rev.*, **1951**, 48(3), 397-541. <http://dx.doi.org/10.1021/cr60151a002>
- [10] Keri, R.S.; Hiremathad, A.; Budagumpi, S.; Nagaraja, B.M. Comprehensive review in current developments of benzimidazole-based medicinal chemistry. *Chem Biol Drug Des.*, **2015**, 86(1), 19-65. <http://dx.doi.org/10.1111/cbdd.12462> PMID: 25352112
- [11] Vitaku, E.; Smith, D.T.; Njardarson, J.T. Analysis of the structural diversity, substitution patterns, and frequency of nitrogen heterocycles among U.S. FDA approved pharmaceuticals. *J Med Chem.*, **2014**, 57(24), 10257-10274. <http://dx.doi.org/10.1021/jm501100b> PMID: 25255204
- [12] Shrivastava, N.; Naim, M.J.; Alam, M.J.; Nawaz, F.; Ahmed, S.; Alam, O. Benzimidazole scaffold as anticancer agent: Synthetic approaches and structureactivity relationship. *Arch. Pharm. (Weinheim)*, **2017**, 350(6), e201700040. <http://dx.doi.org/10.1002/ardp.201700040>
- [13] Shimomura, I.; Yokoi, A.; Kohama, I.; Kumazaki, M.; Tada, Y.; Tatsumi, K.; Ochiya, T.; Yamamoto, Y. Drug library screen reveals benzimidazole derivatives as selective cytotoxic agents for KRAS-mutant lung cancer. *Cancer Lett*, **2019**, 451, 11-22. <http://dx.doi.org/10.1016/j.canlet.2019.03.002> PMID: 30862488
- [14] Haider, K.; Yar, M.S. Advances of benzimidazole derivatives as anti-cancer agents: bench to bedside. *Benzimidazole*; Kendrekar, P.; Adimule, V., Eds.; IntechOpen: London, **2022**. <http://dx.doi.org/10.5772/intechopen.101702>
- [15] Petrov, K.G.; Zhang, Y.M.; Carter, M.; Cockerill, G.S.; Dickerson, S.; Gauthier, C.A.; Guo, Y.; Mook, R.A., Jr; Rusnak, D.W.; Walker, A.L.; Wood, E.R.; Lackey, K.E. Optimization and SAR for dual ErbB-1/ErbB-2 tyrosine kinase inhibition in the 6-furanyloquinazoline series. *Bioorg. Med. Chem. Lett.*, **2006**, 16(17), 4686-4691. <http://dx.doi.org/10.1016/j.bmcl.2006.05.090> PMID: 16777410
- [16] Xie, Z.; Wu, K.; Wang, Y.; Pan, Y.; Chen, B.; Cheng, D.; Pan, S.; Guo, T.; Du, X.; Fang, L.; Wang, X.; Ye, F. Discovery of 4,6-pyrimidinediamine derivatives as novel dual EGFR/FGFR inhibitors aimed EGFR/FGFR1-positive NSCLC. *Eur. J. Med. Chem.*, **2020**, 187, 111943. <http://dx.doi.org/10.1016/j.ejmech.2019.111943> PMID: 31846829
- [17] Okamoto, I. Epidermal growth factor receptor in relation to tumor development: EGFR-targeted anticancer therapy. *FEBS J.*, **2010**, 277(2), 309-315. <http://dx.doi.org/10.1111/j.1742-4658.2009.07449.x> PMID: 19922468
- [18] Chikhale, R.; Thorat, S.; Choudhary, R.K.; Gadewal, N.; Khedekar, P. Design, synthesis and anticancer studies of novel aminobenzazopyl pyrimidines as tyrosine kinase inhibitors. *Bioorg. Chem.*, **2018**, 77, 84-100. <http://dx.doi.org/10.1016/j.bioorg.2018.01.008> PMID: 29342447
- [19] Moyer, J.D.; Barbacci, E.G.; Iwata, K.K.; Arnold, L.; Boman, B.; Cunningham, A.; DiOrto, C.; Doty, J.; Morin, M.J.; Moyer, M.P.; Neveu, M.; Pollack, V.A.; Pustilnik, L.R.; Reynolds, M.M.; Sloan, D.; Theleman, A.; Miller, P. Induction of apoptosis and cell cycle arrest by CP-358,774, an inhibitor of epidermal growth factor receptor tyrosine kinase. *Cancer Res.*, **1997**, 57(21), 4838-4848. PMID: 9354447
- [20] Talambedu, U.; Sushil, K.; Arvind, K.; Mahesh, K.; Da, M.; Syed, F.; Peyush, G.; Hp, P.; Veena, P. Molecular docking studies of anticancerous candidates in Hippophae rhamnoides and Hippophae salicifolia. *J. Biomed. Res.*, **2014**, 28(5), 406-415. <http://dx.doi.org/10.7555/JBR.28.20130110> PMID: 25332713
- [21] Jayaraj, R.L.; Ranjani, V.; Manigandan, K.; Elangovan, N. In-silico docking studies to identify potent inhibitors of alpha-synuclein aggregation in parkinson disease. *Asian J. Pharm. Clin. Res.*, **2013**, 6(4), 127-131.
- [22] Luo, Y.; Deng, Y.Q.; Wang, J.; Long, Z.J.; Tu, Z.C.; Peng, W.; Zhang, J.Q.; Liu, Q.; Lu, G. Design, synthesis and bioevaluation of N-trisubstituted pyrimidine derivatives as potent aurora A kinase inhibitors. *Eur. J. Med. Chem.*, **2014**, 78, 65-71. <http://dx.doi.org/10.1016/j.ejmech.2014.03.027> PMID: 24681066
- [23] Bekker, H.; Berendsen, H.J.C.; Dijkstra, E.J.; Achterop, S.; van Drunen, R.; van der Spoel, D.; Sijbers, A.; Keegstra, H. Gromacs: A parallel computer for molecular dynamics simulations. *Phys. Comp.*, **1993**, 92, 252-256.
- [24] Ganesan, A.; Coote, M.L.; Barakat, K. Molecular dynamics-driven drug discovery: Leaping forward with confidence. *Drug Discov. Today*, **2017**, 22(2), 249-269. <http://dx.doi.org/10.1016/j.drudis.2016.11.001> PMID: 27890821
- [25] Thalla, M.; Kant, K.; Dalchand, ; Rawat, R.; Banerjee, S. Merged experimental guided computational strategy toward tuberculosis treatment mediated by alveolar macrophages mannose receptor. *J. Biomol. Struct. Dyn.*, **2020**, 38(17), 5195-5203. <http://dx.doi.org/10.1080/07391102.2019.1697369> PMID: 31779532
- [26] Schmid, N.; Eichenberger, A.P.; Choutko, A.; Riniker, S.; Winger, M.; Mark, A.E.; van Gunsteren, W.F. Definition and testing of the GROMOS force-field versions 54A7 and 54B7. *Eur. Biophys. J.*, **2011**, 40(7), 843-856. <http://dx.doi.org/10.1007/s00249-011-0700-9> PMID: 21533652
- [27] van Aalten, D.M.F.; Bywater, R.; Findlay, J.B.C.; Hendlich, M.; Hoof, R.W.W.; Vriend, G. PRODRG, a program for generating molecular topologies and unique molecular descriptors from coordinates of small molecules. *J. Comput. Aided Mol. Des.*, **1996**, 10(3), 255-262. <http://dx.doi.org/10.1007/BF00355047> PMID: 8808741
- [28] Mark, P.; Nilsson, L. Structure and dynamics of the TIP3P, SPC, and SPC/E water models at 298 K. *J. Phys. Chem. A*, **2001**, 105(43), 9954-9960. <http://dx.doi.org/10.1021/jp003020w>
- [29] Van Gunsteren, W.F.; Berendsen, H.J.C. A leap-frog algorithm for stochastic dynamics. *Mol. Simul.*, **1988**, 1(3), 173-185. <http://dx.doi.org/10.1080/08927028808080941>
- [30] Berendsen, H.J.C.; van der Spoel, D.; van Drunen, R. GROMACS: A message-passing parallel molecular dynamics implementation. *Comput. Phys. Commun.*, **1995**, 91(1-3), 43-56. [http://dx.doi.org/10.1016/0010-4655\(95\)00042-E](http://dx.doi.org/10.1016/0010-4655(95)00042-E)
- [31] Hess, B.; Bekker, H.; Berendsen, H.J.C.; Fraaije, J.G.E.M. LINCS: A linear constraint solver for molecular simulations. *J. Comput. Chem.*, **1997**, 18(12), 1463-1472. [http://dx.doi.org/10.1002/\(SICI\)1096-987X\(199709\)18:12<1463::AID-JCC4>3.0.CO;2-H](http://dx.doi.org/10.1002/(SICI)1096-987X(199709)18:12<1463::AID-JCC4>3.0.CO;2-H)
- [32] Di Pierro, M.; Elber, R.; Leimkuhler, B. A stochastic algorithm for the Isobaric-Isothermal ensemble with ewald summations for all long range forces. *J. Chem. Theory Comput.*, **2015**, 11(12), 5624-5637. <http://dx.doi.org/10.1021/acs.jctc.5b00648> PMID: 26616351
- [33] Humphrey, W.; Dalke, A.; Schulten, K. VMD: Visual molecular dynamics. *J. Mol. Graph.*, **1996**, 14(1), 33-38, 27-28. [http://dx.doi.org/10.1016/0263-7855\(96\)00018-5](http://dx.doi.org/10.1016/0263-7855(96)00018-5) PMID: 8744570
- [34] Rawat, R.; Kant, K.; Kumar, A.; Bhati, K.; Verma, S.M. HeroMDAnalysis: An automagical tool for GROMACS-based molecular dynamics simulation analysis. *Future Med. Chem.*, **2021**, 13(5), 447-456. <http://dx.doi.org/10.4155/fmc-2020-0191> PMID: 33496197
- [35] Devi, S.; Rangra, N.K.; Rawat, R.; Alrobaian, M.M.; Alam, A.; Singh, R.; Singh, A. Anti-atherogenic effect of Nepitrin-7-O-glucoside: A flavonoid isolated from Nepeta hindostana via acting on PPAR- α receptor. *Steroids*, **2021**, 165, 108770. <http://dx.doi.org/10.1016/j.steroids.2020.108770> PMID: 33227319
- [36] Vaught, A. Graphing with Gnuplot and Xmgr. *Linux Journal*, **1996**. Available from: www.linuxjournal.com/article/1218

DISCLAIMER: The above article has been published, as is, ahead-of-print, to provide early visibility but is not the final version. Major publication processes like copyediting, proofing, typesetting and further review are still to be done and may lead to changes in the final published version, if it is eventually published. All legal disclaimers that apply to the final published article also apply to this ahead-of-print version.